Transactions on Energy Systems and Engineering Applications

Article

An approach for the definition of the thermal regime of buildings for energy saving

Natalia Orlova[1,*] and Svitlana Alyokhina[2]

[1] Department of Modeling and Identification of Thermal Processes in Energy Technology Equipment, Anatolii Pidhornyi Institute of Power Machines and Systems of the National Academy of Sciences of Ukraine, Kharkiv, Ukraine.

[2] Department Industrial Engineering, University of Applied Sciences Technikum Wien, Vienna, Austria.

[*] Correspondence: naorl@ukr.net

Received: 26 June 2024; Accepted: 23 February 2026; Published: 09 March 2026

Abstract: The research presented in this article addresses the critical issue of assessing thermal regimes in buildings and the subsequent development of energy-saving measures. With a focus on the thermal microclimate within urban areas, particularly in response to changing economic conditions and energy consumption patterns, the study investigates external factors influencing building thermal loads. Through a comprehensive methodology, the research explores the interplay between building elements, airflow dynamics, and energy consumption patterns. The study highlights the complexities of building thermal regimes, emphasizing the need for tailored solutions based on individual comfort requirements and environmental conditions. The findings highlight the significance of considering external disturbances, such as wind speed and direction, in assessing building thermal performance. The study provides insights into heat transfer mechanisms, boundary layer dynamics, and airflow distributions around buildings through numerical simulations and experimental validations. The proposed methodology offers a practical approach to enhancing building energy efficiency by optimizing heating systems, refining heat loss calculations, and improving thermal comfort for occupants. By considering a range of factors, from building orientation to external weather conditions, the study advocates for an individualized approach to building energy management, thereby paving the way for sustainable and environmentally conscious building practices.

1. Introduction

Requirements for life-support standards are closely linked to the economic potential of a particular region [1]. For instance, GDP growth in European countries (currently around 0.6%) leads to increased energy consumption in residential, administrative, and industrial buildings [2, 3]. Such a situation necessitates a review and reassessment of building thermal regimes to subsequently develop energy-saving measures.

How to cite this article: Orlova, Natalia; Alyokhina, Svitlana. An approach for the definition of the thermal regime of buildings for energy saving. *Transactions on Energy Systems and Engineering Applications*, 7(1): 701, 2026. DOI:10.32397/tesea.vol7.n1.701

Determining the thermal regime of buildings is a complex task due to the variety of factors influencing the indoor microclimate. Improving the methodology for determining the thermal load of each building within a thermal micro-district requires a systemic approach that describes the relationship between building elements (external walls, glazing), indoor and outdoor air temperatures, and their mutual arrangement, considering wind velocity and building orientation.

Research into individual comfort conditions in residential apartments shows that people living in warm climatic zones prefer a warmer indoor temperature compared to those in cold climatic zones. Statistical analyses of thermal comfort semantics, based on thermal sensations and indoor and outdoor temperature data, show that residents of naturally ventilated buildings tolerate temperature variations over a wider range. This indicates that revising building thermal regime standards is necessary for energy conservation, depending on the individual requirements of occupants [4, 5].

Since centralized heating systems are a crucial part of future intelligent energy systems, new approaches are required to assess their overall energy efficiency. To enable integration of heating systems into broader energy subsystems, models of heat consumption management in centralized heating systems were analyzed [6, 7], along with parameters that have the greatest impact on end-user heat consumption following the implementation of individual metering.

Modeling the thermal regime of buildings for evaluating annual energy balance distributions, assessing compliance with energy standards, and optimizing economic parameters during the design process are other ways to ensure building energy efficiency [8, 9].

For heating and air-conditioning load calculations that require rapid computation with acceptable accuracy, correlation algorithms based on modeling are often used, typically employing commercial 3D software. The simplified approach presented by Ren, Motlagh, and Chen [10] and Balocco and Petrone [11] refines heat loss calculations through foundations and offers simplicity and computational speed. However, to assess overall heat losses, it is still necessary to refine heat exchange parameters and evaluate their variation with climatic conditions.

At the initial stage, assessing the potential for energy savings requires simple methods. For example, the approach outlined in ISO 13789:2017 [12] uses analytical formulas for calculating steady-state heat transfer, derived from empirical data. However, applying this approach requires refinement of certain coefficients characterizing heat exchange between exterior building walls and the surrounding environment. Carreira, Costa, Mansur, and Arsénio [13] proposed a mobile user interface that accounts for variable environmental parameters. The interface models the thermal regime of a building under changing climate conditions. Energy consumption reduction is achieved through a k-means machine learning algorithm, which automatically adjusts the HVAC system while maintaining acceptable indoor microclimate conditions. However, this method cannot be applied to outdated heating systems lacking digital automation.

Combining analytical and experimental methods makes it possible to consider individual space requirements, thus improving energy efficiency by analyzing changes in the thermophysical parameters of building elements under varying external and internal factors. This approach was applied in a study of microclimate parameters in an open-plan office with approximately 50 occupants, resulting in an interactive air-conditioning control system [14]. However, this approach cannot serve as a universal method for assessing building thermal regimes for subsequent energy-saving measure development.

Building services also include electrical networks. An analysis of electricity and heat consumption as a function of outdoor air parameters showed that reducing electricity use generally leads to increased heating loads. Lam, Wan, Tsang, and Yang [15] and Pagliarini, Bonfiglio, and Vocale [16] analyzed the relationship between heating loads and electricity consumption in office buildings across five major climatic zones: severe cold, cold, hot summer/cold winter, mild/hot summer, and warm winter, using building energy modeling.

Qi, Zhang, and Jin [17] proposed a methodology for analyzing the energy-saving potential of thermal insulation and occupant behavior in different climatic zones. Two categories of heating hours dominate the energy-saving mechanism: temperature-difference-saving hours and behavioral-saving hours. The method evaluates energy-saving potential based on occupant behavior but does not consider the thermophysical parameters of building structures, heating systems, external climatic conditions, or indoor microclimate, which is a major limitation.

Sigrimis, Ferentinos, Arvanitis, and Anastasiou [18] conducted a comparative analysis of two algorithms for assessing building thermal regimes:

- The first uses meteorological forecasts to determine heating parameters.
- The second relies on historical data to obtain the desired average for any user-defined period, without requiring weather forecasts.

Modeling results showed that for short integration periods (e.g., 24 h), both algorithms yielded similar energy consumption values, while the first achieved slightly better savings – if forecasts and consumption models were accurate. For longer periods (e.g., 2–3 days), the second method performed comparably and proved more robust under uncertainty, suggesting that analytical methods incorporating refined thermophysical parameters, meteorological data, terrain, and building characteristics are promising.

Implementing energy-saving measures (Figure 1) is a complex multi-stage task requiring initial assessment of heat loss reduction. The relevance of energy saving in residential and public buildings calls for a comprehensive approach that considers not only economic efficiency but also building life cycle, technological feasibility, and stakeholder interests. The proposed framework illustrates the systemic interrelation of organizational, technical, and informational measures that can be integrated during both major renovations and routine maintenance.

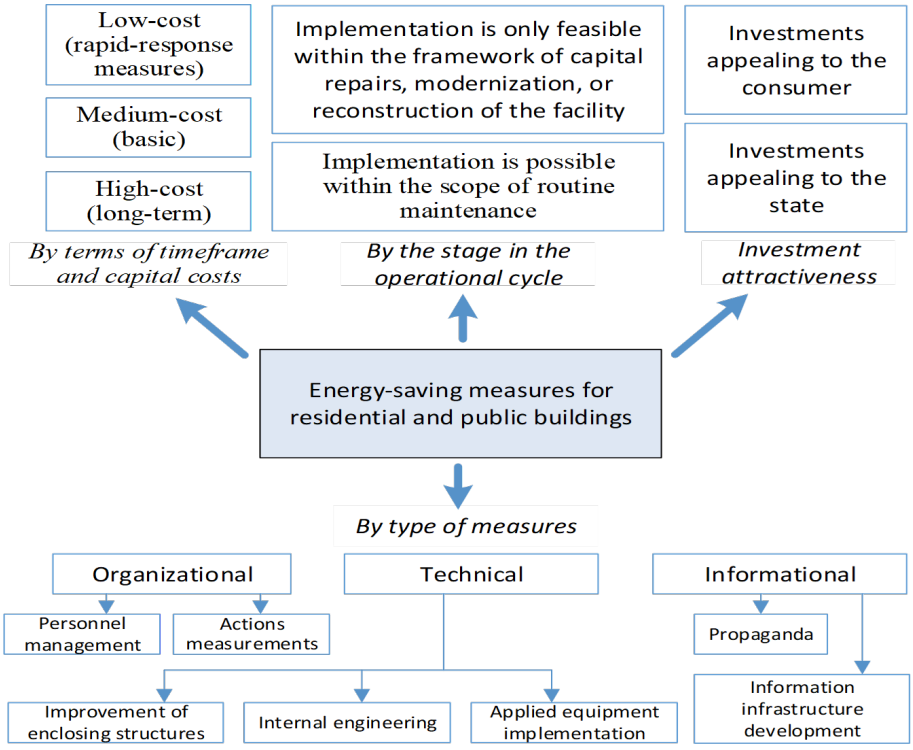

Figure 1. Classification of energy-saving measures.

Sobota and Taler [19] and Najjar, Figueiredo, and Hammad [20] presented numerical algorithms for calculating heat losses through external building elements with air gaps during insulation. These algorithms enable more accurate determination of heat losses and temperature distribution across wall thicknesses but require refinement of the dependence of thermophysical parameters on air humidity, outdoor temperature, and wind conditions.

To refine heat loss estimates, transient states—such as building heating at the start of the heating season and subsequent cooling—must be accurately evaluated, as well as heat gains. Stafford, Bell, and Gorse [21] evaluated solar heat gains, finding that they may periodically repeat, while dynamic solar changes can lead to underestimation of heat losses in steady-state analyses. Inaccurate solar radiation measurements can bias heat loss estimates. Experimental results confirm that solar gains depend on environmental conditions and dwelling characteristics [22].

Mangematin, Pandraud, and Roux [23] assessed heat losses during transient processes, demonstrating their impact on overall building energy efficiency. Since actual heat losses depend on system performance and building envelope characteristics, experimental evaluations were conducted [24,25]. Actual operational losses were determined via transmission and infiltration through the envelope, and an algorithm summing both components was proposed. Assessing infiltration losses is particularly relevant for buildings with heat recovery ventilation.

Due to discrepancies between calculations and real operation, accurate assessment of operational building characteristics is essential for determining energy efficiency classes not only for new constructions but also for modernized ones. Alzetto, Farmer, Fitton, Hughes, and Swan [26] evaluated an experimental method for determining heat losses due to infiltration and transmission. Short measurement durations and incomplete boundary conditions caused discrepancies, underscoring the need for refined boundary indicators and their harmonization with experimental data.

Currently, building energy efficiency is determined using models "tuned" through computational-experimental data. Baasch, Westermann, and Evins [27] created a dataset of 16,000 modeled buildings. While such models are widely used, their scalability and reliability for various property types remain unclear. Moreover, they require separate databases for each city area, unlike analytical algorithms that rely only on experimental data corrected for heat consumption per individual consumer.

2. Problem Formulation

The thermal regime of indoor spaces during the heating season is influenced by variable external and internal disturbances. Internal disturbances include the presence of occupants, household heat emissions, and heat gains from equipment and lighting fixtures. External disturbances comprise fluctuations in outdoor air temperature, wind speed and direction, solar radiation intensity, and air humidity. Compensation for these disturbances is achieved by adjusting the parameters of the heat carrier within the heating system. The operation of a heating system is generally characterized by two dynamic parameters: the temperature of the heat carrier and its flow rate.

For system analysis and optimal control when modeling centralized heating systems, the following steps are required:

- Analysis of external influences, including the prediction of their variations;
- Representation of the control object as a hierarchical structure of sub-systems;
- Analysis of input effects and output parameters for each subsystem at every level;
- Identification of key parameters for each sub-system;
- Harmonization of control criteria across the entire heating system;
- Development of a conceptual control model for the system.

To determine output parameters that ensure the required indoor environmental conditions for consumers and to generate appropriate heat carrier values for the stable operation of technological processes with minimal production and transport costs, it is necessary to analyze control variables, external disturbances, and their variations. Synthesizing a control model for centralized heating systems is complicated by the uncertainty of the system's parameters, including:

- Non-stationarity of system parameters – such as pipeline hydraulic characteristics, the condition of thermal insulation, and building heat losses;
- The stochastic nature of external disturbances;
- Uncertainty of control criteria.

The heating system is characterized by process inertia, including capacitive and transport delays as well as control response delays. Heat waves passing through thermally massive building elements (walls, floors, modern energy-efficient windows) attenuate and exhibit phase lags, resulting in slow heat losses. In contrast, non-massive enclosures exhibit fast heat losses, occurring almost synchronously with temperature fluctuations. Therefore, when managing a centralized heating system, it is necessary to consider not only the complex of meteorological factors but also the changes that occurred during previous periods and those forecasted for the near future [28, 29].

To address the complex tasks of operational management and planning, a functional control scheme for the centralized heating system is proposed (Figure 2). The diagram illustrates a closed-loop control of the thermal regime of buildings, influenced by both external meteorological conditions and the intrinsic characteristics of the buildings. Measured parameters are compared with the setpoints, after which actuators adjust the heat supply accordingly. The control system uses data from heat distribution networks, consumers, and weather forecasts to calculate the optimal distribution of heat flows. This approach ensures a stable indoor climate while minimizing excessive energy consumption.

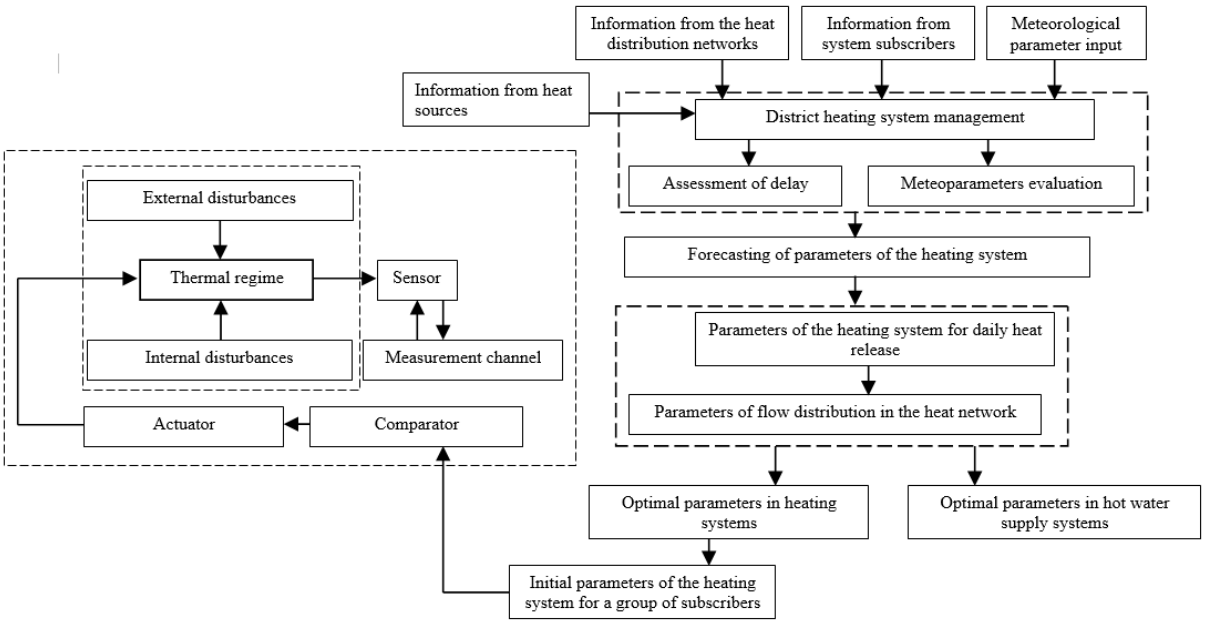

Figure 2. The functional diagram of the operational control system for the district heating system.

According to the functional diagram, operational control is aimed at addressing several interrelated tasks:

- Development of multi-level control models that encompass all stages of the district heating system;
- Formalization and selection of optimization criteria to balance energy efficiency and indoor thermal comfort;
- Synthesis of predictive models for daily heat release and thermal load forecasting;
- Determination of locally adaptive parameters to fine-tune and adjust the thermal regime at the level of individual rooms and zones.

The thermal regime of residential buildings is determined by the indoor air temperature (T_{in}), its movement, and humidity. While the latter two parameters depend on the building's ventilation system, the indoor air temperature (T_{in}) is influenced by climatic conditions (such as outdoor air temperature T_{out}, wind speed, and direction), as well as by the thermal properties of walls, floors, windows, and air exchange within the rooms.

This study examines a typical district in the city of Kharkiv, Ukraine. According to the Program for the Development and Reform of Housing and Communal Services in the City of Kharkiv for 2011–2025 (Resolution No. 328/10 of 27.10.2010, as amended on 24.06.2020), the existing centralized heating system is a large-scale system operating on the principle of constant flow [30]. The system's infrastructure is in poor condition and requires substantial investment. It consists of approximately 400 km of trunk (primary) networks and about 1,100 km of distribution (secondary) networks. In addition, there are around 600 km of hot water supply pipelines laid in the same channels as the heating networks.

The system is designed as a closed and dependent network, without heat exchangers in building heating systems. Space heating is primarily provided through hydroelevators, while domestic hot water is supplied by heat distribution stations. Most of the heating networks pass through these distribution stations — there are 218 in total. As no heat exchangers are installed for heating at these stations, buildings are connected directly via a four-pipe scheme. The heating networks were originally designed for a temperature schedule of 150/70 °C; however, due to the technical condition of the pipelines and the current economic situation, the actual supply temperature rarely exceeds 120 °C.

The existing heating system in Kharkiv follows a typical constant-flow configuration. In this case, centralized regulation is performed at production stations, and fixed heating zones operate under two main constant-flow (and pressure) modes: the winter flow mode and the summer flow mode.

The considered thermal district of Kharkiv has the following characteristics: the heating demand is 17.62 MW, the hot water supply demand is 16.39 MW, and heat losses due to air leakage from infiltration and natural ventilation amount to 0.32 MW. Table 1 presents the structure of this thermal district. The district is predominantly composed of multi-storey residential buildings of standard series. The housing stock includes 25 buildings of series I-464, 7 buildings of series I-438, one building of series A-163, and 16 buildings of series I-447, along with 7 administrative buildings. The largest share of total living area and number of apartments belongs to the I-464 series, which can therefore be considered representative for analyzing the district's thermal regime and for performing detailed numerical modeling of heat supply and loss processes.

Table 1. The structure of the thermal district.

Building type (Series)	Number of buildings	Number of flats	Living area, m^2
I-464	25	2840	158475
I-438	7	770	29981.2
A-163	1	108	6352.2
I-447	16	1278	84001.5
Administrative buildings	7	—	—

During the heating season, the flow rate of the heat carrier at the heat distribution station is approximately 320 tons per hour, with a maximum hot water flow rate of 160 tons per hour. The minimum pressure in the supply pipeline from the HPP is 0.59 MPa, while the maximum pressure in the return pipeline is 0.47 MPa. The hot water temperature is 50 °C. Consumers are connected through 78 automatic heating control nodes. The total length of intra-block heating networks is 5.5 km.

The purpose of this study is to develop an approach for assessing the thermal regimes of buildings under external disturbances, including the calculation of heat transfer coefficients for external building walls, using a thermal district in an old urban area as a case study.

3. Methodology

The object of this study is a residential district in the city of Kharkiv, Ukraine (Figure 3). The city is located at a mean latitude of approximately 50°, which corresponds to a temperate continental climate. This climate is characterized by moderately cold and variable winters, as well as a prolonged summer period that may be dry and hot in some years.

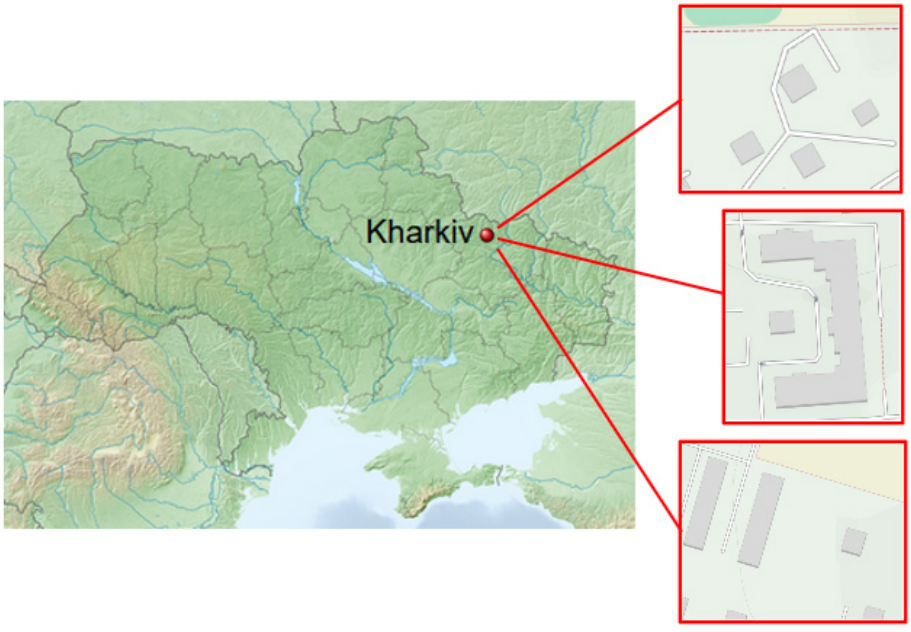

Figure 3. Studied district in Kharkiv (Ukraine).

The mean annual air temperature is 8.1 °C, and the average annual precipitation is approximately 515 mm. Analysis of long-term climatic data indicates that the mean annual temperature in Kharkiv increased by about 0.5 °C between 1970 and 2000.

The wind regime of the city does not exhibit a pronounced prevailing direction. Easterly winds account for approximately 18% of observations, while westerly winds occur in about 16% of cases. Calm conditions are frequent during the summer period. In spring, easterly and south-easterly winds prevail; in summer, north-westerly winds dominate; and in autumn and early winter, westerly winds are most common. During winter, wind directions are distributed almost uniformly.

According to national regulations, the heating season in Ukraine begins when the average daily outdoor air temperature remains below +8 °C for three consecutive days. For Kharkiv, the average duration of the heating season is approximately 180 days.

3.1. General Calculation Framework

The determination of the heating load of building heating systems within the studied thermal district is carried out in a step-by-step manner (Figure 4). In this study, aerodynamic modeling is used as the basis for calculating building heat losses.

The calculation procedure includes the following stages:

- Specification of external climatic conditions, including outdoor air temperature, wind speed, and wind direction;
- Determination of boundary conditions on the external surfaces of building envelopes, taking into account the mutual arrangement of buildings;
- Calculation of heat transfer coefficients for transparent building envelope elements [31];
- Evaluation of heat losses due to infiltration and uncontrolled air leakage;
- Calculation of heating loads based on representative buildings of the studied district.

This sequence ensures a direct link between airflow characteristics around the built environment and the resulting heat losses of buildings.

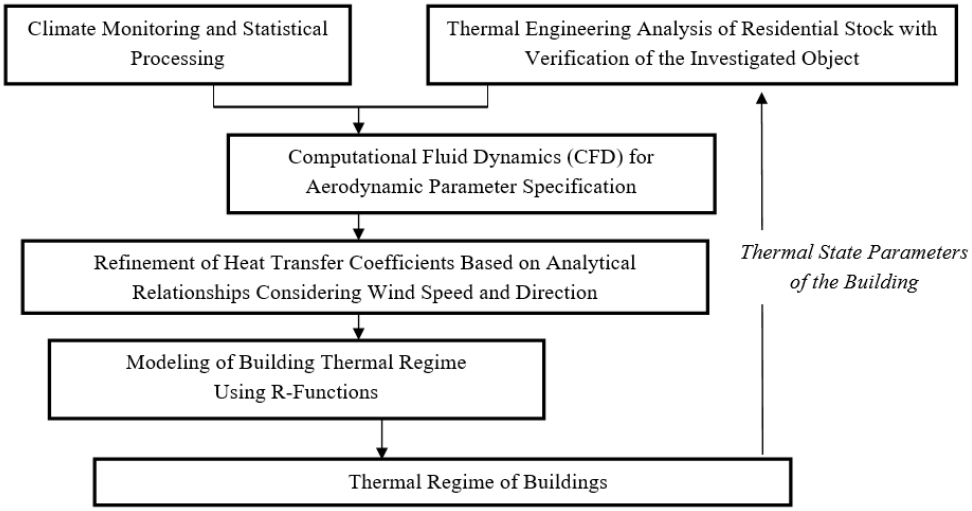

Figure 4. Methodology flowchart.

Thermal processes are modeled under quasi-steady-state conditions. Air humidity and material properties are assumed constant. Indoor air temperature is prescribed according to design conditions. The wind flow is modeled as turbulent. Radiative heat transfer is incorporated via an equivalent heat transfer coefficient. Internal heat gains are included based on design values. The heating system is analyzed in steady-state mode without transient control effects.

Aerodynamic Modeling and Heat Transfer

To determine the heat transfer coefficient on the leeward side of the building, the model incorporates key aerodynamic parameters, including the vertical wind speed profile, the pulsating component of wind velocity, the boundary layer thickness, and the extent of the gradient flow region.

Analysis of the wake structure behind the building, compared with the flow around a flat plate oriented perpendicular to the onset flow, demonstrates a clear aerodynamic similarity. This similarity justifies the application of established correlation dependencies to calculate the average heat transfer coefficients on the windward side of the building.

Analyzing the flow structure behind the building model [32, 33] and the flow conditions around a plate positioned perpendicular to the airflow, a similarity between these cases can be observed. Therefore, to calculate the average values of the heat transfer coefficients on the windward side of the building, the following correlation can be applied:

$$\mathrm{Nu}_{av} = 0.0207 \cdot \mathrm{Re}_{av}^{2/3}, \tag{1}$$

where Nusselt number $\mathrm{Nu}_{av} = \dfrac{\alpha_{out}^{lw} \cdot L}{\lambda_{av}}$, and Reynolds number $\mathrm{Re}_{av} = \dfrac{U_0\, L}{v_{av}}$, L – building length, m; v_{av} – air kinematic viscosity, m^2/s; U_0 – the wind speed in front of a buildings' group, m/s.

In this context, the building length is defined as the characteristic linear dimension, while the flow velocity is taken as the wind speed upstream of the building cluster. Given the negligible temperature gradient between the wall surface and the ambient air, coupled with relatively low flow velocities, the thermophysical properties of the air are assumed to be constant and consistent with ambient environmental conditions.

Heat Transfer on the Leeward Side of the Building

The distribution of the aerodynamic coefficient over the building façade is characterized by a local behavior corresponding to the flow stagnation zones, which allows for the use of appropriately averaged heat transfer coefficients in the calculations. For the leeward side of the building, the heat transfer coefficient is determined through a simplified relationship that accounts for the thermal conductivity of air:

$$\alpha_{\mathrm{lee}} = 0.47 \cdot \frac{\lambda}{L} \cdot Re^{0.5}, \tag{2}$$

where λ – air thermal conductivity, W/(m·K).

4. Results and discussion

To verify the results and extend their applicability to various urban patterns, parametric CFD simulations were performed using the OpenFOAM software package [34]. Based on the data obtained, the impact of building geometry on the airflow velocity field was generalized, providing a basis for developing predictive dependencies.

The numerical simulation results established the wind velocities for a group of buildings. It was found that the transformation of the wind flow under urban development conditions is a key factor influencing the thermal regime of the structures. Figures 5 and 6 visualize the velocity contours at a height of 2 meters above ground level for both isolated buildings and clusters. Meanwhile, the relative geometric parameters are expressed as:

$$\overline{H_1} = H_1 / H_2; \tag{3}$$

$$\overline{L_1} = L_1 / H_2; \tag{4}$$

$$\overline{\Lambda_1} = \Lambda_1 / H_2; \tag{5}$$

where Λ_1 – the distance between buildings, measured from the tall building, m; Λ_2 – the distance between low-rise buildings, m; L_1 –the length of the tall building, m; L_2 – the length of the low-rise building, m.

The results are visualized as iso-velocity contours (isotachs):

- Figure 5 shows the isotachs of relative air velocities in the near-ground zone (with a grid step of $H/2$).
- Figure 6 presents the isotachs of relative velocities at a critical height of 2 m above ground level (the grid step is also $H/2$).

The resulting airflow distribution enables the determination of locally adjustable parameters required for fine-tuning the thermal regimes of individual rooms within the operational control system.

Figure 5 illustrates the iso-velocity contours in the near-ground zone for different building configurations. The upper part depicts the velocity distribution behind a single building of height $H_1/H_2 = 2$, where a recirculation zone forms in the leeward area and the flow velocity gradually recovers with increasing distance. The analysis also considers the airflow around a system of two buildings of different heights ($H_1/H_2 = 2$), located at distances of $\Lambda_1/L_1 = 0.5$ and $\Lambda_2/L_2 = 0.5$, respectively. In this case, the relative positioning of the buildings significantly affects the flow field structure, leading to the formation of extended low-velocity regions, localized recirculation zones, and a distorted airflow distribution behind the buildings.

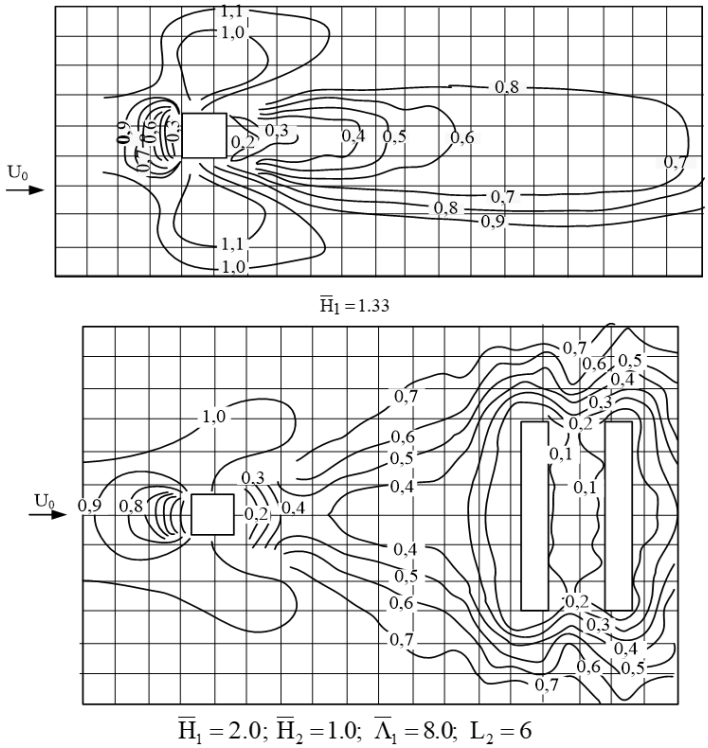

Figure 5. The iso-speed lines of relative air velocities in the ground-level area (grid step equals H_2).

Such modifications in the airflow structure reflect the influence of building density and spacing on the characteristics of the near-ground atmospheric layer and must be considered when modeling microclimatic conditions and heat exchange processes in residential districts.

Figure 6 presents the iso-velocity contours of relative airflow at a height of 2 m above ground level for a group of low-rise buildings, characterized by the relative building height ($\overline{L_2'} = 4$) and the relative spacing between them ($\overline{\Lambda_1} = 4$). At $\varphi = 90$, when the flow is oriented perpendicularly to the extended façade, zones of accelerated flow are formed near the windward corners ($U/U_0 \approx 0.9$–1.1), while extended stagnant regions with reduced velocity $U/U_0 \approx 0.1$–0.3) appear on the leeward side. In the inter-facade spaces, defined by the relative ratio (a $\overline{\Lambda_1} = 4$), a shielding effect is observed, where the relative velocity decreases below 0.2.

At $\varphi = 45$, the general aerodynamic zoning remains similar, but the spatial distribution is rearranged: accelerated jets shift along the lateral façades, recirculation zones are displaced toward the leeward corners, and inter-building passages—defined by the same relative parameter ($\overline{\Lambda_1} = 4$), develop jet-like flows with increased velocities. Thus, under constant relative parameters ($\overline{\Lambda_1} = 4$), the aerodynamic structure retains its main features, while the angle of attack determines the specific configuration and intensity of the zones, directly influencing façade heat transfer and the microclimatic conditions in the surrounding urban area.

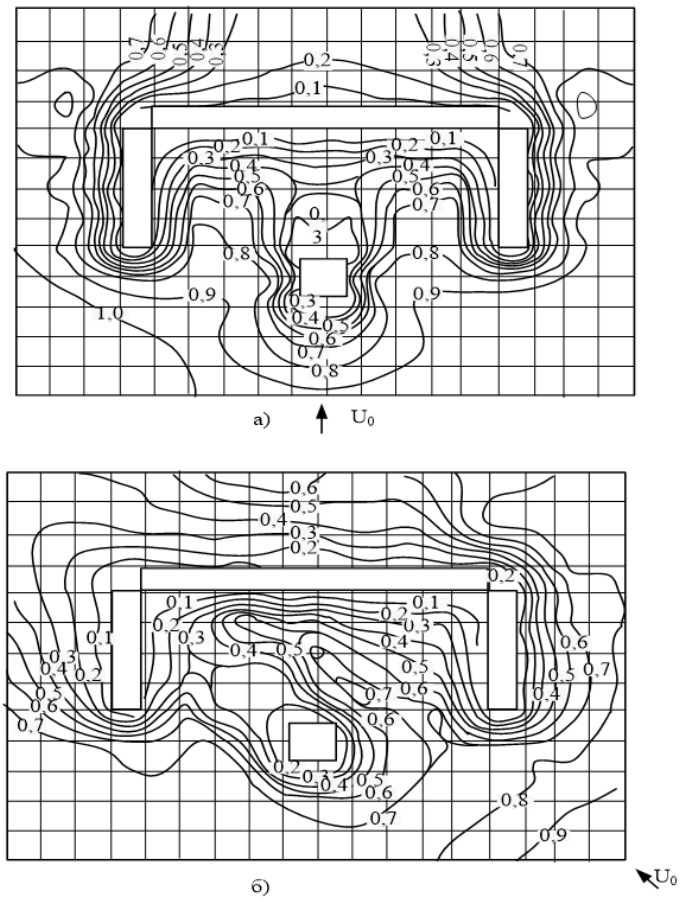

a) $\overline{H}_2 = 2,\ \overline{L}_2 = 10,\ \overline{L}_2' = 4,\ \overline{\Lambda}_1 = 4,\ \varphi = 90^0$
b) $\overline{H}_2 = 2,\ \overline{L}_2 = 10,\ \overline{L}_2' = 4,\ \overline{\Lambda}_1 = 4,\ \varphi = 45^0$

Figure 6. The iso-speed lines of relative air velocities at a height of 2 m above ground level (grid spacing is equal to H2).

Given the diversity of building layouts, it is necessary to generalize the influence of parameters characterizing their mutual arrangement on the airflow distribution. This generalization is required to derive mathematical relationships that make it possible to determine airflow velocities for buildings in various urban configurations. Based on the data presented in Figures 5 and 6, the airflow velocity distribution within a group of buildings has been determined.

To identify the parameters of airflow deformation induced by a standalone building, and based on the analysis of aerodynamic flow results presented by Kuznetsov, Butova, Pospíšil (2016) [32], and Michalcova, Kuznetsov, Pospíšil (2014) [33], the following dependencies were obtained:

$$\varphi = 26 + 8.79 \cdot \overline{H}_1^{0.7} \tag{6}$$

$$40.26 \leq \varphi \leq 55 \tag{7}$$

$$\overline{U}_c = 0.8 + 0.26 \cdot \overline{H}_1 \tag{8}$$

$$\bar{l}_{m_{0.5}} = 4.34 \cdot \overline{H}_1 \tag{9}$$

$$1.33 \leq \overline{H}_1 \leq 6.67 \tag{10}$$

where the angle φ, characterizes the direction of the vector of maximum velocity $\overline{U}_c$ at the beginning of the zone of increased velocities, the maximum relative velocity $\overline{U}_c$ in the lateral zone of increased velocities, the length of the separation behind the leeward side of the building $\bar{l}_{m_{0.5}}$, adopted according to the position of the relative velocity in the separation region $\overline{U}_m = 0.5$; $\overline{H}_1$ – the relative width of the tall building B, which was taken as $\overline{H}_1 = H_1/B$ or if $L = B$, H_1 can be represented as $\overline{H}_1 = H_1/L$.

As an example, consider the velocity distribution along the building height (Figure 5(a)). The heat transfer coefficient on the inner surface of the exterior wall was taken as α_{out}=7.3 W/(m^2·K), wall thickness δ=0.35 m, thermal conductivity λ=0.37 W/(m·K), and indoor air temperature T_{out} = 21.5 °C. The duration of the time interval for outdoor air temperature variation is 12 hours (two intervals within a day), with T_{out} = -20 °C and T_{out} = -15 °C; U_0 = 5 m/s, and the wind incidence angle is 90°.

The variation of wind speed with height is calculated according to the dependency

$$U(h) = U_0 \left(\frac{\delta_{b.1}}{h_0}\right)^{n_0} \left(\frac{h}{\delta_{b.1}}\right)^{n}, \tag{11}$$

where U_0 – is the wind speed at height h_0; h_0 - the height of the anemometer on the weather station; n – the exponent, which depends on the type of terrain for which the speed is calculated $U(h)$; n_0 – the exponent that depends on the type of terrain where the anemometer of the weather station is located; $\delta_{b.1}$ – boundary layer thickness.

The exponent values are assumed to be the same as those for large urban centers (since both the weather station and the buildings under study are located in the city center) and are taken as n = n_o = 0.33. To determine the heat transfer coefficient on the windward side of the building, it is necessary to calculate the length of the flow deceleration zone and the boundary layer region, as described by Brdlik and Savin (1965) [35].

The position of the section where the transition from the gradient to the non-gradient region occurs is determined according to the dependency:

$$x_* = 36.153 \cdot \left(\frac{U_0}{\nu}\right)^{0.268} \cdot 0.0828^{1.268} \cdot \left(\frac{\nu}{U_0}\right)^{0.143} \tag{12}$$

or

$$x_* = 1.535 \cdot \left(\frac{U_0}{\nu}\right)^{\frac{1}{8}}. \tag{13}$$

The extent of the boundary layer at a velocity of U_0= 5 m/s, temperature t = 0 °C, and barometric pressure P = 0.0981 MPa x_* =7.6 m. Therefore, for a building length of 52.5 m the width of the deceleration zone will be L_{dec}=L - 2·l_b=38.76 m.

The wind velocity pulsation component is determined as per the following relationship:

$$U' = 0.3 \cdot U_0 \left(\frac{h}{h_0}\right)^n. \tag{14}$$

The calculation results are presented in Table 2.

As seen from Table 2, $U' < 6.5$ m/s, therefore, the heat transfer coefficient in the flow deceleration region can be determined accordingly:

$$\alpha_{out}^{dec} = A \cdot U' \tag{15}$$

where value A = 23.85 J/(m^3·K) is assumed based on the results of an investigation of a flat jet impinging on an obstacle.

Table 2. Key thermal-physical parameters on the windward side of the building.

Floor	$U(h)$, m/s	U', m/s	α_{dec}, W/(m^{2}K)	α_{grad}, W/(m^{2}K)
1	1.25	0.374	8.93	6.32
2	1.608	0.482	11.5	8.15
3	1.86	0.558	13.31	9.42
4	2.05	0.616	14.68	10.39
5	2.21	0.664	15.83	11.21

The table presents the calculated values of key thermophysical parameters on the windward façade of the building as a function of height. As the floor level increases, the flow velocity over the façade surface rises from 1.25 m/s at the first-floor level to 2.21 m/s at the fifth floor. Concurrently, the fluctuating velocity components intensify, indicating an increase in turbulent fluctuations in the upper sections of the building.

These changes directly affect heat transfer processes: both the average and maximum heat transfer coefficients increase with elevation. Specifically, the heat transfer coefficient in the flow deceleration region rises from 8.93 W/(m^2·K) to 15.83 W/(m^2·K), while in the gradient region, it increases from 6.32 W/(m^2·K) to 11.21 W/(m^2·K).

The results indicate that the building's thermal losses are unevenly distributed along the façade and are dependent on elevation. Lower floors are characterized by lower flow velocities and, consequently, less intense heat transfer, whereas upper floors experience more pronounced cooling. This highlights the necessity of specialized adjustments to thermal regimes, accounting for height differentiation, and confirms the feasibility of an individualized approach to managing the building's thermal protection and heat supply.

Considering the mean integrated value of the heat transfer coefficient, represented as:

$$\bar{\alpha} = \frac{1}{x_*} \cdot \int_0^1 \bar{\alpha}(\bar{x}) d\bar{x} = 0.708 \cdot \alpha_{out}^{dec} \tag{16}$$

and Equation (15) the average heat transfer coefficient in the boundary layer flow region according to the data in Table 2 could be found as

$$\alpha_{out}^{grad} = 0.708 \cdot \alpha_{out}^{dec} = 5.066 \cdot U(h). \quad (17)$$

The heat transfer coefficient on the lateral surface of the building is determined by considering the height of the separation region. Based on experimental data provided by Kuznetsov, Butova, and Pospíšil(2016) [32], and Michalcova, Kuznetsov, and Pospíšil (2014) [33], and observations of the flow conditions around multi-story buildings, H_o is taken as H_o=10 m, where the height of the separation region is h_{sep}= 0.434 [36]. With the building width y = 11.95 m, the ratio y/h_{sep} is found in the separated flow region $(y/h_{sep} = 2.75 < 7)$. Therefore, the heat transfer coefficient on the lateral surface of the building is determined by the formula

$$\alpha_{out}^{l} = 0.115 \cdot \rho \cdot U_{sep} \left(\bar{y} + 5\right), \quad (18)$$

where $\bar{y} = \dfrac{y}{h_{sep}}$, with consideration $U_D = 1.41 \cdot U_0$ according to the dependency:

$$\alpha_{out}^{l} = 0.162 \cdot \rho \cdot U_0(0.23 \cdot y + 5). \quad (19)$$

The calculation results are presented in Table 3.

Table 3. Heat transfer coefficients on the exterior lateral surface of the building (α_{lat}, W/(m^{2}K)).

Outer conditions	y, m			
	3	6	9	11.95
$T_{out} = -20$ °C, $\rho = 1.402$ kg/m^3	6.5	7.2	8.0	8.8
$T_{out} = -15$ °C, $\rho = 1.376$ kg/m^3	6.3	7.1	7.9	8.64

The analysis of the calculated data presented in Table 3 demonstrates a pronounced positive gradient of the heat transfer coefficient (α_{out}^{l}) along the vertical coordinate (y) of the building's lateral surface. The observed increase in α_{out}^{l} with increasing y is attributed to the physical regularities governing the development of the atmospheric boundary layer flow and correlates with the rise in the mean velocity of the surrounding flow and the intensity of turbulent pulsations at greater heights.

Quantitative analysis confirms this relationship:

- For the external air temperature regime T_{out}=-20 °C (ρ=1.402 kg/m^3), the heat transfer coefficient increases from 6.50 W/(m^2·K) to 8.80 W/(m^2·K) as the coordinate shifts from 3.0 m to 11.95 m.
- A similar growth in α_{out}^{l} is observed in the external air temperature regime T_{out}=-15 °C (ρ=1.376 kg/m3), increasing from 6.30 W/(m^2·K) to 8.64 W/(m^2·K) within the same coordinate range.

Thus, the absolute increase in the intensity of convective heat exchange along the façade's height ranges from 35.4% to 37.1%, depending on the external conditions. The marginal exceedance of α_{out}^{l} values in the T_{out}=-20 °C regime at identical vertical coordinates are explained by the increased air density. The obtained results convincingly demonstrate a significant vertical non-uniformity of convective heat losses across the building's external surface. This effect necessitates the application of a differentiated approach to thermal design and individualized management of the energy regime for multi-story structures.

The value of the heat transfer coefficient on the leeward side of the building is given in Table 4.

Table 4. Heat transfer coefficients on the leeward side of the building (α_{lee}, W/(m^{2}K)).

Outer conditions	L, m				
	10	20	30	40	52.5
$T_{\text{out}} = -20$ °C, $\lambda = 0.0228$, $\nu_{av} = 11.953 \times 10^{-6}$	1.2	0.94	0.82	0.75	0.68
$T_{\text{out}} = -15$ °C, $\lambda = 0.0231$, $\nu_{av} = 12.4 \times 10^{-6}$	1.2	0.93	0.81	0.74	0.67

Table 4 presents the calculated values of the heat transfer coefficient on the external leeward façade of the building α_{out}^{lw} as a function of the longitudinal coordinate (L) along the surface. The analysis also accounts for variations in the key thermophysical characteristics of the airflow, including outdoor air temperature T_{out}, thermal conductivity λ, and kinematic viscosity v_{av}, enabling a comprehensive assessment of convective heat transfer processes in the recirculation zone.

The results reveal a pronounced negative longitudinal gradient of (α_{out}^{lw}) with increasing coordinate (L) (from 1.0 m to 52.5 m). This behavior is attributed to the dynamics of the aerodynamic wake region, where the decay of velocity and turbulence intensity leads to a reduction in convective heat exchange.

At the initial separation zone (L=1.0 m), the heat transfer coefficient reaches its maximum of approximately (1.20 W/(m^2·K)), while at the end of the interval it decreases to (0.68–0.67 W/(m^2·K)). Overall, the longitudinal reduction in heat transfer intensity amounts to about 43–44%.

The influence of outdoor temperature variations and related changes in thermophysical air properties on the absolute values of α_{out}^{lw} is marginal. This indicates that in the recirculation zone the dominant factor is the hydrodynamic flow structure – the configuration and scale of the vortex wake – whereas thermodynamic properties play only a secondary role.

The analysis demonstrates a pronounced longitudinal non-uniformity of thermal losses on the leeward façade. The most intensive heat exchange occurs in the separation zone and near the building edges, while the central part of the wake region is characterized by a sharp decrease in convective intensity. This finding underscores the necessity of a differentiated approach to façade thermal protection and the regulation of heating regimes, considering the distribution of the heat transfer coefficient along the façade's length.

At the considered wind speed, natural convection becomes the determining factor influencing heat exchange on the leeward side. Consequently, the distribution of heat transfer coefficients on the building's exterior façade was determined based on refined calculated dependencies, which account for the local characteristics of airflow velocity and direction obtained through Computational Fluid Dynamics (CFD).

The R-functions Method was employed to provide an analytical description of the complex geometry of the building envelope. Using this method and incorporating the dependencies derived above, the heat transfer coefficients were determined (Figure 7) and subsequently applied in the thermal calculations. The final solution to the heat transfer boundary value problem, aimed at determining the required temperature of the heating appliances (Figure 8), was also implemented using the R-functions Method. This approach allowed the heterogeneous field of heat transfer coefficients (Figure 8) to be integrated into the boundary value problem, enabling the determination of locally adjustable parameters necessary for optimizing the thermal regime of individual premises [37].

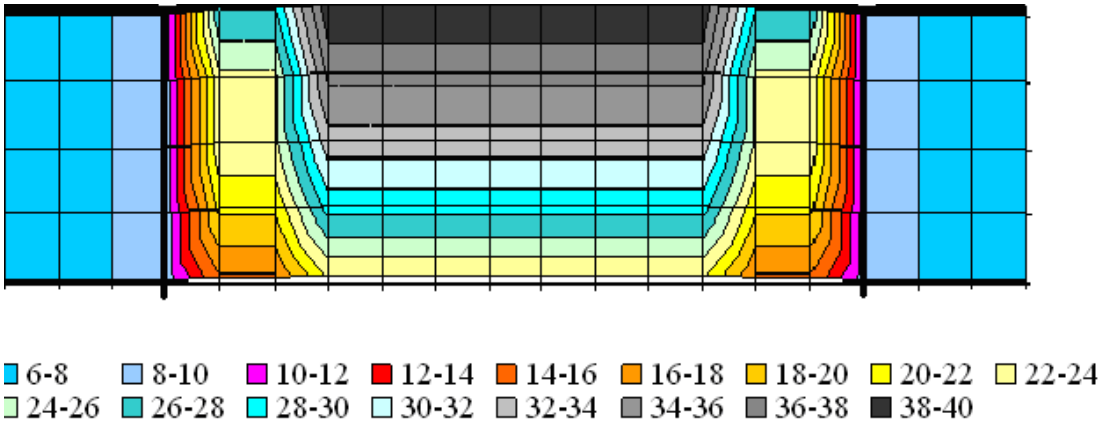

Figure 7. Distribution of heat transfer coefficient on the building exterior walls.

Figure 7 illustrates the distribution of the heat transfer coefficient (α) on the external surface of the building. The values range from 6–8 to 38–40 W/(m^2·K), indicating pronounced spatial non-uniformity of heat exchange.

A clear vertical gradient is observed: from the lower part of the surface (6–10 W/(m^2·K), corresponding to a flow deceleration zone) to the upper part (up to 38–40 W/(m^2·K), associated with intensive interaction with the atmospheric boundary layer). Additional edge effects are identified: along the lateral boundaries, the coefficient increases due to flow acceleration and the formation of vortex structures.

At a fixed height, horizontal non-uniformity is also evident, with α increasing from the central axis towards the lateral zones, particularly in the middle and upper parts of the surface. This reflects the three-dimensional nature of the flow and the localized intensification of heat exchange.

Thus, the greatest heat losses occur in the upper and corner zones of the external surface, which confirms the necessity of differentiated thermal protection measures to improve the energy efficiency of buildings. Such differences in heat transfer coefficients on the external surfaces lead to a significant temperature variation inside the building, depending on the floor and the direction of the airflow ingress.

The variation in temperature of the heat source depending on the floor, considering the orientation of the room towards the cardinal directions and the number of external surfaces, is shown in Figure 8.

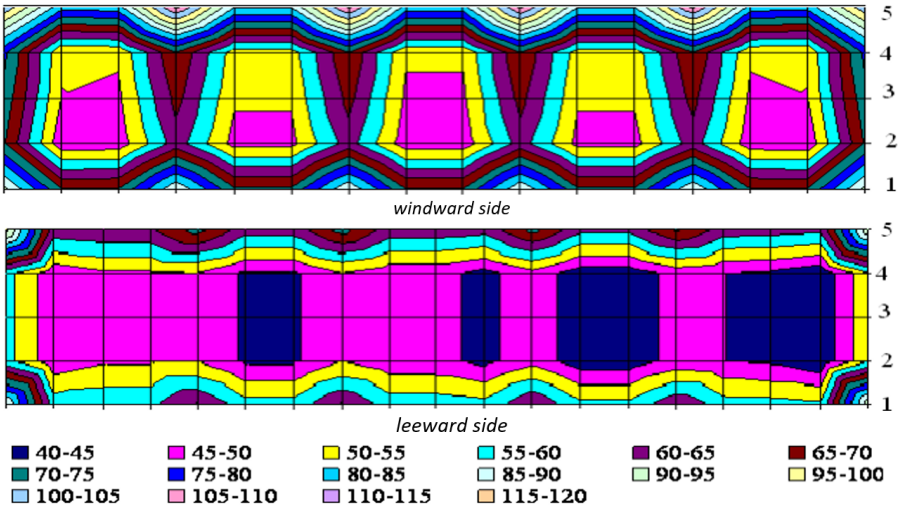

Figure 8. Distribution of temperature (°C) of heating elements in the 5-story building.

The distribution of coolant temperatures in heating units (Figure 8) of a five-story building is determined by the wind flow vector, the number of stories, and the thermal heterogeneity of the building envelope. On windward façades, the intensification of convective heat transfer on external surfaces leads to an increase in thermal load. Maximum temperature values (95°–115°C) are recorded in corner rooms, as well as on the ground and top floors, due to additional heat losses. On the leeward side, as a result of reduced aerodynamic influence, unit temperatures in central zones range from 45° to 60°C. An increase in values to 65°–85°C is observed only in the peripheral zones of the façade. Thus, a significant spatial non-uniformity of the building's temperature field has been established, caused by the difference in specific thermal loads between windward and leeward sections.

Experimental and theoretical studies confirm the necessity of accounting for local aerodynamic coefficients when calculating heat supply systems. According to the developed methodology, the estimated daily thermal load for a typical I-464A series building amounted to $Q'_o(24)$ = 3296 kWh/day (α_{out}=23 W/(m^2·°C), α_{in}=7.3 W/(m^2·°C)). The total load for the studied district heating area is $\Sigma Q'_o(24)$ =356927 kWh/day (the characteristics of this thermal region are presented in Table 1).

Refining thermo-technical parameters by considering the aerodynamic characteristics of airflow interaction allows for a 15% reduction in the estimated thermal energy demand. For the residential sector of Kharkiv (under the conditions of the 2020–2021 heating season), the potential savings amount to approximately 982 thousand Gcal per season.

4.1. Comparative analysis of normative and CFD-based approaches

In [38], external convective heat transfer coefficients are provided in the form of recommended ranges derived from empirical correlations for isolated flat plates and simplified building geometries. Typical recommended values range from approximately 5 to 40 W/m^2·K depending on wind conditions, without explicit consideration of façade orientation, height-dependent wind profiles, or urban aerodynamic interactions.

In contrast, [39] adopts a fixed external surface resistance (α_{out}=0.04 m^2·K/W), corresponding to a constant convective heat transfer coefficient of 25 W/m^2·K, independent of wind speed, building geometry, or urban morphology.

The convective heat transfer coefficients are in good agreement with full-scale experimental data reported by Vasiliev (1957) [40], with deviations within 5–10% (Table 5). This confirms the adequacy of the numerical modeling approach and the physical consistency of the aerodynamic heat transfer representation.

Table 5. Comparison of external convective heat transfer coefficients α_{out}, W/(m^{2}K).

This study, W/(m^2·K)	Vasilyev (1957) [40], W/(m^2·K)	ASHRAE [38], W/(m^2·K)	ISO 6946 [39], W/(m^2·K)
18–25	17–23	5–40	25
8–14	7–13	5–40	25
25–40	23–37	5–40	25
22–30	20–28	5–40	25
15–22	14–20	5–40	25

Normative approaches exhibit fundamental methodological limitations. In [39] a constant external heat transfer coefficient is assumed, while [38] provides broad recommended ranges without accounting for façade orientation, vertical wind stratification, or urban aerodynamic interactions. As a result, normative coefficients fail to reproduce the spatial heterogeneity of convective heat transfer observed in real urban environments.

Figure 9 presents the variation of heating source temperature with floor level and façade orientation. The CFD results are compared with full-scale measurements reported by Vasilyev (1957) [40].

The results demonstrate pronounced vertical and orientation-dependent variations in heating source temperatures. Upper floors and windward façades require higher supply temperatures due to intensified wind-driven convective heat losses, whereas leeward façades exhibit systematically lower heating demand. Deviations between numerical and experimental data remain within 10–15%, indicating satisfactory model validation.

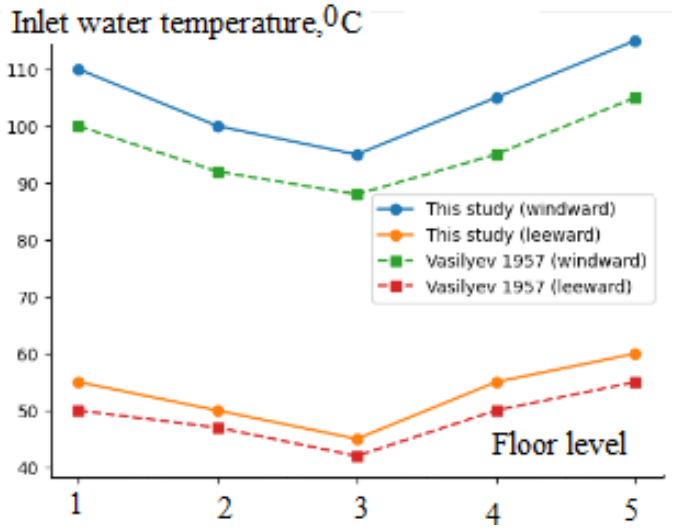

Figure 9. Vertical distribution of heating source temperature (comparison with Vasilyev, 1957) [40].

The I-464-3 building series represents typical mass housing construction of the 1960s–1970s, with heights not exceeding 15 m for five-storey and 27 m for nine-storey configurations. Normative heat transfer models were historically developed for such low- and mid-rise buildings, whereas modern high-rise urban environments exhibit fundamentally different aerodynamic flow regimes and convective heat transfer patterns. Therefore, direct extrapolation of conventional coefficients to contemporary urban buildings introduces significant uncertainties.

This implies that normative heat transfer coefficients derived for historical low-rise building stock are not transferable to contemporary high-rise urban environments without substantial physical and methodological revisions.

The comparison reveals that normative heating design approaches implicitly assume spatially uniform boundary conditions, which contradict both simulations and full-scale measurements. ASHRAE and ISO 6946:2017 standards neglect building-scale aerodynamic effects, leading to systematic underestimation of heating demand for windward and upper-floor zones and overestimation for leeward zones [38, 39]. This explains the widely observed phenomenon of simultaneous overheating and underheating in centralized heating systems.

By incorporating façade- and height-dependent convective heat transfer coefficients, the proposed methodology provides a physically grounded framework for spatially differentiated heating control. This approach enables improved prediction of heating loads and supports next-generation district heating optimization strategies.

The results demonstrate that the use of spatially uniform convective heat transfer coefficients, as adopted in current ASHRAE and ISO 6946:2017 standards [38, 39], is insufficient for dense urban environments.

Incorporating urban aerodynamic effects into thermal models is therefore essential for accurate heating load prediction and advanced district heating system control.

5. Conclusions

This study aimed to enhance the methodological approach to assessing the thermal performance of buildings by incorporating external disturbances and refining the heat transfer coefficients of enclosing structures. A typical residential district of old urban development was used as a case study.

The scientific novelty of this study lies in the fact that, for the first time in district heating research, building-scale aerodynamic characteristics of airflow are employed for the simultaneous description of façade heat losses and the formation of individual indoor heating temperature regimes at the level of separate rooms. In contrast to existing studies on district heating optimization, which typically rely on constant or empirically averaged heat transfer coefficients, this work demonstrates that airflow aerodynamics around buildings—governed by their orientation, height, and urban layout—has a substantial impact on the spatial and temporal distribution of façade heat losses. The proposed approach refines thermal load assessment by introducing dynamically varying heat transfer coefficients and enables the systematic identification of underheating and overheating zones that are not captured by conventional models.

The developed methodology, which sequentially considers climatic parameters (outdoor air temperature, wind speed, and direction), refines the boundary conditions for building envelopes and adjusts heat transfer coefficients to account for infiltration processes and airflow interaction with external surfaces, enabling a comprehensive assessment of heat losses and the spatial distribution of temperature regimes in residential buildings.

The analysis revealed a pronounced spatial heterogeneity in thermal regimes. On windward façades and in apartments located on the first and top floors, the highest heating element temperatures (95–115 °C) were recorded. These elevated temperatures were attributed to increased heat transfer coefficients and additional heat losses through ground and roof structures. In contrast, on leeward façades, heat losses were significantly lower, resulting in heating element temperatures as low as 45–60 °C in central rooms, with increases up to 65–85 °C only in corner zones and on extreme floors.

The scientific novelty of the study lies in the development of a refined algorithm for assessing building heat losses that accounts for:

- Local effects of airflow interaction with external surfaces;
- Orientation-dependent differentiation of building zones (windward, leeward, lateral);
- Floor-dependent variability in thermal regimes.

For the first time, it has been demonstrated that incorporating airflow interaction characteristics into thermal regime modeling not only improves the accuracy of heating load assessments but also enables the identification of critical zones of overheating and underheating. This is essential for optimizing the performance of heat supply systems.

The practical significance of the results lies in the potential application of the proposed approach for adaptive regulation of indoor thermal regimes, mitigation of overheating and underheating effects, and reduction of total heat consumption in the residential sector by up to 15% during the heating season.

Future research directions include the integration of dynamic climate scenarios, refinement of infiltration models, and the development of intelligent district- and city-scale heating control systems. These efforts aim to create a foundation for energy-efficient strategies in the context of climate change and aging urban infrastructure.

Funding: This research received no external funding.

Author contributions: Conceptualization, S.A. and N.O.; Methodology, N.O.; Software, N.O.; Validation, N.O.; Formal Analysis, N.O.; Investigation, N.O.; Resources, N.O.; Data Curation, N.O.; Writing – Original Draft Preparation, S.A. and N.O.; Writing – Review & Editing, S.A.; Visualization, N.O.; Supervision, S.A.; Project Administration, S.A.; Funding Acquisition, S.A.

Disclosure statement: The authors declare no conflict of interest.

References

[1] IEA EBC. Total energy use in buildings – analysis and evaluation methods. *Energy and Buildings*, 2017. Annex 53.

[2] M. Bourdeau, X. Zhai, E. Nefzaoui, X. Guo, and P. Chatellier. Modeling and forecasting building energy consumption: A review of data-driven techniques. *Sustainable Cities and Society*, 48:101533, 2019.

[3] H. Gao, C. Koch, and Y. Wu. Building information modelling based building energy modelling: A review. *Applied Energy*, 238:320–343, 2019.

[4] M. Humphreys and F. Nicol. Understanding the adaptive approach to thermal comfort. *ASHRAE Transactions*, 104(1):991–1004, 1998.

[5] R. de Dear and G. S. Brager. Developing an adaptive model of thermal comfort and preference – final report on RP-884. *ASHRAE Transactions*, 104(1), 1997. Report no. RP-884.

[6] D. Maljkovic and B. D. Basic. Determination of influential parameters for heat consumption in district heating systems using machine learning. *Energy*, 201:117585, 2020.

[7] E. T. Al-Shammari et al. Prediction of heat load in district heating systems by support vector machine with firefly searching algorithm. *Energy*, 95:266–273, 2016.

[8] Ž. Turk. Ten questions concerning building information modelling. *Building and Environment*, 107:274–284, 2016.

[9] G. Mutani and V. Todeschi. Building energy modeling at neighborhood scale. *Energy Efficiency*, 13(7):1353–1386, 2020.

[10] Z. Ren, O. Motlagh, and D. Chen. A correlation-based model for building ground-coupled heat loss calculation using artificial neural network techniques. *Journal of Building Performance Simulation*, 13(1):48–58, 2019.

[11] C. Balocco and G. Petrone. Numerical modelling for the thermal performance assessment of a semi-opaque façade with a multilayer of nano-structured and phase change materials. *Buildings*, 7(4):90, 2017.

[12] ISO 13789:2017. thermal performance of buildings – transmission and ventilation heat transfer coefficients – calculation method, 2017.

[13] P. Carreira, A. A. Costa, V. Mansur, and A. Arsénio. Can HVAC really learn from users? a simulation-based study on the effectiveness of voting for comfort and energy use optimization. *Sustainable Cities and Society*, 41:275–285, 2018.

[14] Y. Murakami, M. Terano, K. Mizutani, M. Harada, and S. Kuno. Field experiments on energy consumption and thermal comfort in the office environment controlled by occupants' requirements from PC terminal. *Building and Environment*, 42(12):4022–4027, 2007.

[15] J. C. Lam, K. K. W. Wan, C. L. Tsang, and L. Yang. Building energy efficiency in different climates. *Energy Conversion and Management*, 49(8):2354–2366, 2008.

[16] G. Pagliarini, C. Bonfiglio, and P. Vocale. Outdoor temperature sensitivity of electricity consumption for space heating and cooling: An application to the city of milan, north of italy. *Energy and Buildings*, 204:109512, 2019.

[17] X. Qi, Y. Zhang, and Z. Jin. Building energy efficiency for indoor heating temperature set-point: Mechanism and case study of mid-rise apartment. *Buildings*, 13(5):1189, 2023.

[18] N. Sigrimis, K. P. Ferentinos, K. G. Arvanitis, and A. Anastasiou. A comparison of optimal greenhouse heating setpoint generation algorithms for energy conservation. *IFAC Proceedings Volumes*, 34(11):61–66, 2001.

[19] T. Sobota and J. Taler. Determination of heat losses through building partitions. *MATEC Web of Conferences*, 240:05030, 2018.

[20] M. K. Najjar, K. Figueiredo, A. W. A. Hammad, V. W. Y. Tam, A. C. J. Evangelista, and A. Haddad. A framework to estimate heat energy loss in building operation. *Journal of Cleaner Production*, 235:789–800, 2019.

[21] A. Stafford, M. Bell, and C. Gorse. Building confidence – a working paper. Technical report, Leeds Metropolitan University, 2012.

[22] S. Stamp, R. Lowe, and H. Altamirano-Medina. An investigation into the role of thermal mass on the accuracy of co-heating tests through simulations & field results. In *Building Simulation Conference Proceedings*, 2013.

[23] E. Mangematin, G. Pandraud, and D. Roux. Quick measurements of energy efficiency of buildings. *Comptes Rendus. Physique*, 13(4):383–390, 2012.

[24] H. P. Díaz-Hernández, P. R. Torres-Hernández, K. M. Aguilar-Castro, E. V. Macias-Melo, and M. J. Jiménez. Data-based RC dynamic modelling incorporating physical criteria to obtain the HLC of in-use buildings: Application to a case study. *Energies*, 13(2):313, 2020.

[25] I. Uriarte, A. Erkoreka, A. Legorburu, K. Martin-Escudero, C. Giraldo-Soto, and M. Odriozola-Maritorena. Decoupling the heat loss coefficient of an in-use office building into its transmission and infiltration heat loss coefficients. *Journal of Building Engineering*, 43:102591, 2021.

[26] F. Alzetto, D. Farmer, R. Fitton, T. Hughes, and W. Swan. Comparison of whole house heat loss test methods under controlled conditions in six distinct retrofit scenarios. *Energy and Buildings*, 168:35–41, 2018.

[27] G. Baasch, P. Westermann, and R. Evins. Identifying whole-building heat loss coefficient from heterogeneous sensor data: An empirical survey of gray and black box approaches. *Energy and Buildings*, 241:110889, 2021.

[28] A. Penkovskii. Hierarchical management model of heat supply to consumers. *E3S Web of Conferences*, 219:03004, 2020.

[29] Z. Liu, H. Zhang, Y. Wang, X. Fan, S. You, and A. Li. Data-driven predictive model for feedback control of supply temperature in buildings with radiator heating system. *Energy*, 280:128248, 2023.

[30] The program for the development and reform of housing and communal services in the city of kharkiv for 2011–2025, 2010. Approved by the Kharkiv City Council Session on October 27, 2010 (Resolution No. 328/10), with latest amendments introduced on June 24, 2020 (Resolution No. 2191/20).

[31] V. Malyarenko, S. Alyokhina, and N. Orlova. Methodology for determining heat losses through translucent construction. *Problems of the Regional Energetics*, 3(59):83–98, 2023.

[32] S. Kuznetsov, A. Butova, and S. Pospíšil. Influence of placement and height of high-rise buildings on wind pressure distribution and natural ventilation of low- and medium-rise buildings. *International Journal of Ventilation*, pages 1–14, 2016.

[33] V. Michalcova, S. Kuznetsov, and S. Pospíšil. Numerical and experimental models of load on buildings from the effects of the atmospheric wind. *Advanced Materials Research*, 969:280–287, 2014.

[34] OpenFOAM Foundation. OpenFOAM: The open source CFD toolbox. https://www.openfoam.com/. Accessed: Oct. 10, 2023.

[35] P. M. Brdlik and V. K. Savin. Heat transfer between an axisymmetric jet and a plate normal to the flow. *Journal of Engineering Physics*, 8:91–98, 1965.

[36] N. Orlova and S. Alyokhina. Identification of the flow parameters of separation area near the building corner. *International Journal of Fluid Mechanics Research*, 48(2):47–54, 2021.

[37] K. V. Maksimenko-Sheyko, R. A. Uvarov, and T. I. Sheyko. The R-functions method in mathematical modeling of convective heat transfer in fuel cartridge with fuel rods. *Problems of Atomic Science and Technology*, (3(85)), 2013.

[38] ASHRAE. *ASHRAE Handbook — Fundamentals*. American Society of Heating, Refrigerating and Air-Conditioning Engineers, Atlanta, 2017.

[39] ISO 6946:2017. building components and building elements — thermal resistance and thermal transmittance — calculation method, 2017.

[40] B. F. Vasiliev. *Naturnye issledovaniya temperaturno-vlazhnostnogo rezhima zhilykh zdaniy [Field Studies of the Temperature and Humidity Conditions of Residential Buildings]*. Stroyizdat, Moscow, 1957.